CHEMICAL ENGINEERING TRANSACTIONS
VOL. 59, 2017
A publication of AIDIC
The Italian Association of Chemical Engineering
Online at www.aidic.it/cet
Guest Editors: Zhuo Yang, Junjie Ba, Jing Pan

ISBN 978-88-95608- 49-5; **ISSN** 2283-9216
DOI: 10.3303/CET1759008

Comparative Analysis of Structure and Mechanical Properties of Kavler-49 and Heterocyclic Para-aramid Fibers

Yingdeng Song*, Liying Xing

Beijing Institute of Aeronautical Materials, Beijing 100095, China
songyingdeng@163.com

The F-3 is a traded name of a new type of heterocyclic para-aramid fibers. The relationship between structural parameters and mechanical properties of F-3 has been investigated compared with the Kevlar-49 and Armos. The results showed that the tensile properties of F-3 were higher than those of Kevlar-49 and Armos, resulting from the higher orientation of chains and lower procrystalline parameter for F-3. Based on the results of tensile recoil test, the compressive strength of F-3, Kevlar-49, and Armos was approximate within experimental error. It is suggested that the combination of orientation parameter and shear modulus between adjacent chains results in the approximate compressive strength of F-3, Kevlar-49, and Armos.

1. Introduction

The para-aramid fibers have been widely used as the reinforcement of advanced composite materials in aviation and space engineering due to their low density, high strength, high modulus and thermal stability. There are two different types of para-aramid fiber. One is the poly (p-phenylene terephthalamide) (PPTA) fiber, such as Kevlar and Twaron. The other is the heterocyclic para-aramid (PHA) fiber, such as SVM and Armos (Hearle, 2001). The relationship between structure parameters and tensile properties of PPTA fibers has been reported in detail (Northolt and Baltussen, 2002, Rao et al., 2001). Although the fine structures of PHA fibers have been determined (Zavadskii et al., 2011), there have been few reports on the relation between structure and mechanical properties of PHA fibers (Yang, 2016). In addition, the para-aramid fibers have poor compressive properties compared with other high-performance fibers (e.g. Carbon fiber), which has been limiting their application (Hearle, 2001). It is well known that the intermolecular interaction affects the compressive properties of PPTA fibers (Deteresa et al., 1984, Kozey et al., 1995). In addition, Bazhenov et al. (Bazhenov et al., 1989) have found that the compressive strength of PHA and PPTA fibers was same, suggesting that the intermolecular interaction of PHA fibers is not stronger than that of PPTA fibers, which is different from the findings reported by Abbronin et al. (Abbronin et al., 2002). The F-3 is a traded name of a recently developed type of PHA fibers in China. The structure of the F-3 can be described as a two-phase structure of crystalline and amorphous phase (Wang et al., 2012), which is different from Armos (PHA) considered as a principally non-crystalline structure (Levchenko et al., 1999; Obaid et al., 2011).
In this study, the structural parameters of F-3 was characterized. The intermolecular interaction was simulated. Then, the tensile and compressive properties of single fiber were determined mechanical testing and tensile recoil method, respectively. Finally, the relationship between the structure and mechanical properties of F-3 was discussed in detail. The results may be useful for improving the properties of PHA fibers.

2. Material and method

2.1 Materails

Three kinds of para-aramid fibers (F-3, Kevlar-49 and Armos) were used in this study. The Kevlar-49 (PPTA) was supplied by DuPont. The F-3 (PHA) was provided by China Blue Star Chengrand Chemical Co. Ltd. The Armos (PHA) was developed at Khimvlokno Scientific-Industrial Association in Russia. The value of density is 1440 $kg \cdot m^{-3}$ for Kevlar-49 and F-3, and is 1450 $kg \cdot m^{-3}$ for Armos according to the suppliers.

Please cite this article as: Yingdeng Song, Liying Xing, 2017, Comparative analysis of structure and mechanical properties of kavler-49 and heterocyclic para-aramid fibers, Chemical Engineering Transactions, 59, 43-48 DOI:10.3303/CET1759008

2.2 Structural parameters

2.2.1 Structural parameters of crystallites.

The wide-angle X-ray diffraction (WAXD) was used to characterize the microstructure parameters including equatorial X-ray diffraction crystallinity (*X*), apparent crystal sizes (*ACS*), paracrystalline parameter (g_{II}), and Herman's orientation (f_c). These parameters were obtained according to equatorial and meridional scans, using a PANalytical X'Pert PRO X-ray diffractometer with Ni filter and CuKα radiation (the wavelength λ=0.154 nm). The equatorial scans were performed using the normal-transmission geometry, and meridional scans were collected using $\theta/2\theta$ symmetrical-transmission geometry. .

The equatorial X-ray diffraction crystallinity (*X*) can be defined as ratio of the integrated intensity of a diffraction peak and the integrated intensity of the amorphous peak (Rao et al., 2001). The apparent crystal sizes (ACS) of (*hkl*) were determined using the Scherrer's equation ($L_{hkl}=k\lambda/B^2\cos\theta$, where k=0.9, B is the full-width at half-maximum intensity width of the *hkl* plane). Zavadskii et al. (Zavadskii et al., 2011) have reported the Scherrer's equation can be used to determine the size of the longitudinal ordering zones of Armos.

The paracrystalline parameter (g_{II}) was obtained using following equation (Rao et al., 2001)

$$\beta^2 = \frac{1}{L_{hkl}} + \frac{(\pi g_{II})^4 n^4}{d^2} \tag{1}$$

where β is the broadening of the diffraction peak, L_{hkl} the crystal size, n the order of the diffraction peak, and d the spacing of the first order of the diffraction plane.

2.2.2 Chain modulus and shear modulus

The chain modulus along chain direction (E_c) and shear modulus between adjacent chains (g) were determined using the continuous-chain model (Northolt et al., 2005). This model can be represented using the following equation

$$\frac{1}{E_s} = \frac{1}{E_c} + \frac{\langle \sin^2 \varphi \rangle_E}{2g} \tag{2}$$

where E_s is the sonic modulus ($E_s=\rho C^2$), and $\langle \sin^2\varphi \rangle_E$ the orientation parameter. The sonic modulus of these fibers was measured using the sonic velocity method. Aside from F-3, three different other F-3 fibers (designated F-3A, F-3B, and F-3C) obtained using different process conditions were used in this study. The F-3A is the old version of F-3. The F-3B was obtained by drawing F-3A at high temperature. The F-3C was manufactured by drawing F-3 at high temperature. The reciprocal of the sonic modulus ($1/E_s$) for each fiber was plotted against the value of $\langle \sin^2\varphi \rangle_E$. After the linear regression analysis was carried out, the values of E_c and g were determined according to intercept and slope of the regression line, respectively.

2.2.3 Hydrogen bonds

A molecular-level simulation was used to analyze the hydrogen bonds between adjacent chains for PHA and PPTA. The PPTA segments were built according to the method of Grujicic et al. (Grujicic et al., 2010) The PBIA segment was built by optimizing the conformation by using Condensed-phase Optimized Molecular Potentials for Atomistic Simulation Studies (COMPASS) force field in the software of Material Studio 7.0 (MS). The resulting molecular configuration was optimized by minimizing its potential energy with respect to the positions of the constituent atoms. The perfect PBIA chain segments which had a maximum number of hydrogen bonds were built. The hydrogen bonds in adjacent chain segments were determined using the Hydrogen Bonds Calculation model of MS in which maximum hydrogen-acceptor distance of 4 angstrom was selected in order to obtain the maximum amount of hydrogen bonds between PBIA chain segments.

2.3 Mechanical properties

All the mechanical tests performed in this study were on single fibers. Mechanical testing of para-aramid fibers was performed using an Instron 3345 testing machine at room temperature. For each type of aramid fibers, more than 50 filaments were tested. The fiber diameter was the average of the 50 fibers, measured using SEM.Tensile modulus and tensile strength were determined following the ISO Standard 11566: 1996 (E). The gauge length was 25 mm and the cross-head speed was 10 %·min^{-1}. The griping effects were corrected by adjusting the gauge length. Compressive strength (σ_c) was obtained using the tensile recoil method which has been described in detail by Allen (Allen, 1987).

3. Results and discussion

3.1 Structure parameters

The equatorial and meridional scans of three aramid fibers were shown in Figure 1. As shown in Figure 1 (a), the significant difference in equatorial and meridional diffraction curves indicates the pronounced anisotropy of these fibers. Kevlar fiber was used as the comparison sample. The equatorial scattering curves for Armos fiber, indicating the absence of rigorous order in the position of the molecular chains in the direction perpendicular to the fiber axis. In addition, it can be seen that the scan profile of F-3 was different from that of Armos. The meridional scans of Kevlar-49, Armos and F-3 are shown in Figure 1 (b). It can be seen the F-3 had sharper and higher meridional diffraction peaks than Kevlar-49 and Armos.

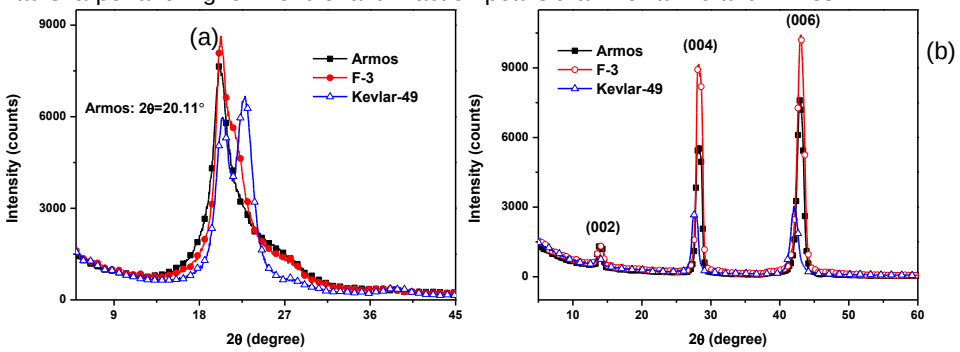

Figure 1: Typical diffraction scans for aramid fibers used: (a) equatorial scans; (b) meridional scans.

Equatorial scans of F-3 and Kevlar-49 were fitted using the Gaussian function and resolved into three peaks and an amorphous peak(Wang et al., 2012, Peng et al., 2005). The structure parameters can be calculated by using the data in Figure 1. The results are given in Table 2 where the values of ACS of F-3 were close to those of Kevlar-49, and the X and gII of F-3 were lower than those of Kevlar-49.As shown in Figure 1 (b), meridional scans for these fibers were characterized by intense narrow diffraction reflections, indicates high longitudinal ording of their structure. The results of orientation parameter $\langle sin^2\varphi \rangle_E$ indicated that molecular chains of F-3 have a higher degree of orientation in longitudinal direction.

Table 1: Microstructure parameters of aramid fibers

Fiber	X^*/%	ACS/nm			g_{II}^{**}/%	$\langle sin^2\varphi \rangle_E$
		L_{110}	L_{200}	L_{002}		
Kevlar-49	81.40	5.1	4.9	9.6	2.48	0.0471
F-3	75.88	5.9	4.1	10.7	2.10	0.0069
Armos	-	-	-	10.5	-	0.0102

* Crystallinity. ** Paracrystalline parameter. *** f_c is orientation of crystalline, amorphous, and average orientation of molecular chains, respectively. ACS: apparent crystal sizes

As shown in Table 1, F-3 has a relatively high equatorial crystallinity. Analyzing the crystalline structure of other types of F-3 using WAXD, Wang et al. (Wang et al., 2012) have found the crystallinity decreases with the increasing proportion of PBIA segments and the pure PBIA fiber is amorphous. Thus, F-3 has a high proportion of PPTA segments and a low proportion of PBIA segments compared with Armos, so that it has a relatively high crystallinity.

Although the structural parameters in transverse direction of fiber, L_{110} and L_{200} of F-3 and Kevlar-49 were approximate within experimental error, L_{110} was larger and L_{200} was smaller for F-3 compared with Kevlar-49. The L_{110} was enlarged due to steric effect caused by PBIA units. When it is drawn in the special spinning process and treated by heat, the more macromolecules in F-3 keep a stress-holding state (Wang et al., 2012). Thus, the chain conformation is transformed into the more stretched *trans*-conformation for PPTA units in F-3, resulting in the L_{200} decreased. The decreased L_{200} leads to more hydrogen bonds between adjacent chains within the plane parallel to (100), so that the crystallites of F-3 may have a more perfect 2_1 symmetries along *c*-axis (Rao et al., 2001).

In addition, L_{002} of F-3 was larger than that of Kevlar-49, and closed to that of Armos as shown in Table 2, suggesting that the size of the longitudinal ordering zones in F-3 was larger than that of Kevlar-49 and Armos. Rao et al. (Rao et al., 2001) have found that large longitudinal crystallite size is associated with low paracrystalline parameters (g_{II}). It is suggested that the large longitudinal crystallite size and low g_{II} for F-3

result from the high orientation of chains, which is demonstrated by the relationship among the values of $\langle sin^2\varphi \rangle_E$, L_{002}, and g_{II}.

3.2 Modulus

3.2.1 Tensile modulus

The results of tensile and compressive testing for F-3, Armos and Kevlar-49 are given in Table 2. The tensile modulus and strength of F-3 were both higher than those of Armos and Kevlar-49. For F-3, large size of crystallites in fiber axis (L_{002}) and low paracrystalline parameter (g_{II}) are also associated with the high tensile modulus (Table 1 and Table 2). Rao et al. (Rao et al., 2001) have proposed that the tensile modulus increases with the decrease of $\langle sin^2\varphi \rangle_E$ and g_{II}, which is in accord with the data of F-3 shown in Table 1 and Table 2.

Table 2. The mechanical properties of para-aramid fibers

Fiber	Tensile strength/GPa	Tensile modulus/GPa	Beak elongation/%	Compressive strength/MPa
Kevlar-49	3.04±0.33	106±5.5	3.38±0.23	425±42
F-3	4.69±0.32	158±5.3	3.81±0.30	462±42
Armos	4.31±0.37	139±7.2	4.10±0.34	438±32

3.2.2 Chain modulus

In order to determine the chain modulus (E_c) and shear modulus (g) between adjacent chains of F-3, the reciprocal of the sonic modulus ($1/E_s$) for different F-3 fibers was plotted against the value of orientation ($\langle sin^2\varphi \rangle_E$) (Figure 2). These data were fitted by linear regression. The E_c of about 223 GPa was obtained according to the intercept of the regression line, and the g of about 1.0 GPa was determined according to the slope of regression line. Northolt's line (Northolt et al., 2002) was also plotted in Figure 2 by using equation (2). The continuous-chain model, equation (2), to adequately describe the modulus of highly oriented fibers has been used to analyze the relationship between modulus and orientation (Northolt et al., 2005).The chain modulus of F-3 (E_c=223 GPa) is slightly less than of PPTA fiber (E_c=240 GPa) reported (Northolt et al., 2002) (Table 3). Perepelkin (Perepelkin, 2004) has reported the range of theoretical chain modulus of PHA fibers is 220-240 GPa. Thus, it is suggested that the chain modulus of 223 GPa for F-3 is acceptable.

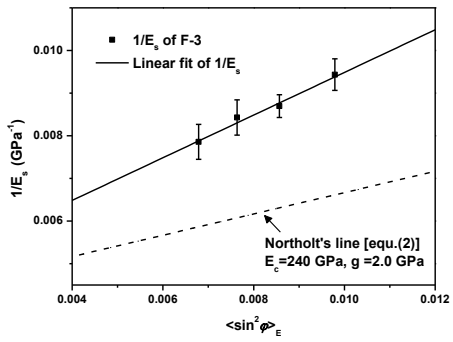

Figure 2: Variation of the reciprocal of sonic modulus for F-3 fibers $1/E_s$ with $\langle sin^2\varphi \rangle_E$.

3.2.3 Shear modulus

Shear modulus between adjacent chains (g) of F-3 has been determined according to Figure 2. For highly oriented fibers without crack fiber, shear modulus is approximately equal to g (Northolt et al., 2002) . It can be seen that F-3 had a lower value of g than Kevlar-49, indicating that the intermolecular interaction between the chains is weak for F-3 compared with PPTA fiber. Evidently, the hydrogen bonds are primarily contributor of intermolecular interaction in highly oriented polymer fibers.

To analyze the intermolecular interaction of PHA and PPTA fibers, the PPTA and PBIA chain segments were simulated using the Material Studio 7.0 software. The simulation results of perfect molecular chains in PBIA segments are shown in Figure 3 (a), and the molecular chains in PPTA segments are shown in Figure 3 (b). It can be seen that the maximum number of hydrogen bonds between adjacent chains in perfect PBIA segments was smaller than in PPTA segments, indicating that the number of hydrogen bonds was smaller for PHA (F-3, Armos) than for PPTA (Kevlar-49).As shown in Figure 3 (a), even though the distance of adjacent chains of PBIA segments was set to equal to *b*-dimension of PPTA unit cell (5.18 angstrom), the distance between N in

PBIA segment and H in amino group of adjacent molecular chain was still larger than 4 angstrom, indicating that the hydrogen bonds cannot form. In fact, the distance of adjacent chains may be larger in real PBIA segments, suggesting that the number of hydrogen bonds in real PHA fiber may be smaller than in simulated ones. Furthermore, the molecular chains in real PBIA segments are absence of the perfect alignment shown in Figure 3 (a), so that hydrogen bonds in PHA are less than in PPTA fiber. Thus, it is suggested that the intermolecular interaction of F-3 is weaker than that of PPTA fiber. F-3 has a lower shear modulus than PPTA fiber because of its weak intermolecular interaction.

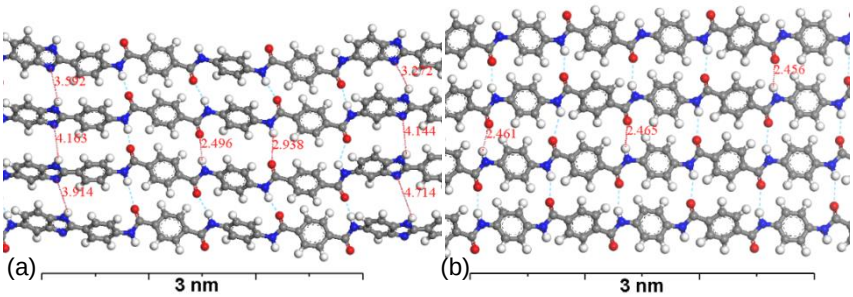

Figure 3: The hydrogen bonds between adjacent chains of PBIA (a) and PPTA (b) segments obtained by molecular simulation. (The short dash lines represent hydrogen bonds.)

3.3 Compressive Strength

The compressive strengths (σ_c) determined by tensile recoil method for F-3, Armos, and Kevlar-49 are given in Table 2. In addition, the values of σ_c for F-3A, F-3B, and F-3C were 458±35 MPa, 420±40 MPa, and 416±46 MPa, respectively. The results showed that the value of σ_c for F-3 was approximately close to that for Armos and Kevlar-49 within experimental error.

Although different structures of para-aramid fibers had different tensile properties, there was no significant difference in the compressive strength (σ_c) of F-3, Armos, and Kevlar-49. Our results are consistent with those reported previously for PPTA and PHA fibers (Kozey et al., 1995, Bazhenov et al., 1989). It is generally accepted that the intermolecular interaction affects the compressive property. In this case, a relation, based on yield mechanism of highly oriented-polymeric fibers, was used to analyze σ_c of F-3, which can be expressed as (Northolt et al., 2002)

$$\sigma_c = \frac{2g\gamma}{\sqrt{\langle \sin^2\varphi \rangle_E}\sqrt{1-\langle \sin^2\varphi \rangle_E}} \quad (3)$$

where γ is the yield strain (γ≈0.025), φ the orientation angles of an equivalent zig-zag bundle of aligned parallel chains in a fiber. Figure 4 shows the values of σ_c of different F-3 fibers plotted against the values of $\langle sin^2\varphi \rangle_E$. The lines in Figure 4 have been calculated from equation (3) using values of g=1. 0 GPa for F-3, and g=2. 0 GPa for PPTA (Northolt et al., 2002). There are evidently differences in experimental data and theoretical curves because the values of $\langle sin^2\varphi \rangle_E$ employed is not enough to provide a critical test of the equation (3). This also may be because the theory is not strictly correct or, more likely, due to difficulties in obtaining the values of $\langle sin^2\varphi \rangle_E$ free from error. Even so, it is suggested that the compressive strength of para-aramid fibers is determined by the combination of the orientation parameters and shear modulus between adjacent chains (Figure 4). Thus, the combination of high orientation along the fiber axis and weak intermolecular interaction results in the approximate compressive strength of F-3 and Kevlar-49.

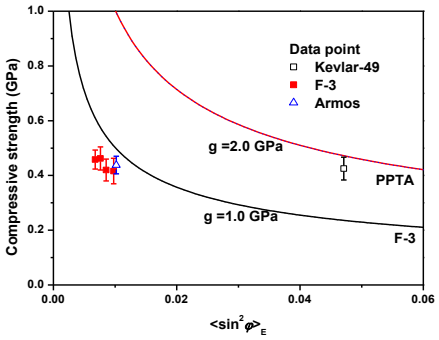

Figure 4: Dependence of the compressive strength upon orientation parameter. The theoretical lines have been calculated from equation (13) using g=1.0 GPa for F-3 fiber and g=2.0 GPa for PPTA fiber.

4. Conclusion

The structural parameters and mechanical properties of F-3 have been investigated compared with Armos and Kevlar-49. The results showed that the tensile properties of F-3 were higher than those of Armos and Kevlar-49. The compressive strengths determined by recoil method for F-3, Armos and Kevlar-49 was approximate. Our experimental results suggest that chain modulus and shear modulus for F-3 are lower than for Kevlar-49. In addition, the combination of orientation parameter and shear modulus results in the approximate compressive strength of F-3, Armos and Kevlar-49. The results of this present study give a unique insight into the relationship between structure and mechanical properties in para-aramid fibers, especially for PHA fibers. They should enable further advances to analyze the failure mechanism of aramid fiber reinforced resin composites.

Reference

Abbronin I.A., Rakitina V.A., Gribanov V.A., 2002, Quantum Chemical Calculation of the Character of Structural Organization and H-Bond Energy in the Benzimidazole Fragment of Fibres of the Armos Type, Fibre Chem, 34(2), 140-145. DOI: 10.1023/A:1016372929610.

Allen S.R., 1987, Tensile Recoil Measurement of Compressive Strength for Polymeric High-Performance Fibres, Journal of Materials Scienc, 22(3), 853-859, DOI: 10.1007/BF01103520.

Bazhenov S.L., Kozey V.V., Berlin A.A., 1989, Compression Fracture of Organic Fibre Reinforced Plastics, Journal of Materials Science 24(12), 4509-4515.

Chen C.F., Lan J., Peng T., 2014, The development situation, preparation, properties and applications of Russian aramid fibers, Hi-Tech Fiber & Appl., 39(1), 26-31.

Deteresa S.J., Allen S.R., Farris R.J., 1984, Compressive and Torsional Behaviour of Kevlar 49 Fibre. Journal of Materials Science, 19(1), 57-72, DOI: 10.1007/BF00552994.

Grujicic M., Bell W.C., Glomski P.S., 2010, Filament-Level Modeling of Aramid-Based High-Performance Structural Materials, Journal of Materials Engineering and Performance, 2011, 20(8), 1401-1413, DOI: 10.1007/s11665-010-9786-y

Hearle J.W.S., 2001, High-Performance Fibres. Cambridge: Woodhead Publishing Ltd, 115-132.

Kozey V.V., Jiang H., Mehta V.R., 1995, Compressive Behavior of Materials: Part II, High Performance Fibers, J. Mater. Res. 10, 4, 1044-1061.

Levchenko A.A., Antipov E.M., Plate N.A., 1999, Comparative Analysis of Structure and Temperature Behaviour of Two Copolyamides - Regular Kevlar and Statistical Armos. Macromol. Symp. 146(1), 145-151.

Northolt M.G., Blatussen J.J.M., 2002, The Tensile and Compressive Deformation of Polymer and Carbon Fibers. Journal of Applied Polymer Science, 2002, 83 (3), 508-538, DOI: 10.1002/app.2256.

Northolt M.G., Den Decker P., Picken S.J., 2005, The Tensile Strength of Polymer Fibres. In: Polymeric and Inorganic Fibers: Springer Berlin Heidelberg, 1-108.

Obaid A.A., Deitzel J.M., Gillespie J.W., 2011, The Effects of Environmental Conditioning on Tensile Properties of High Performance Aramid Fibers at near-Ambient Temperatures. Journal of Composite Materials, 2011, 45(11), 1217-123, DOI: 10.1177/0021998310381436.

Perepelkin K.E., 2004, Theory of Extremal Mechanical and Thermal Properties of Fibres and Needle Crystals, Comparison with Experimental Data. Fibre Chem. 36(4), 237-248.

Rao Y., Waddon A.J., Farris R.J., 2001, Structure–Property Relation in Poly (P-Phenylene Terephthalamide) (PPTA) Fibers. Polymer. 42(13), 5937-5946, DOI: 10.1016/S0032-3861(00)00905-8

Wang F.D., Chen C.F., Peng T., 2012, Structure and properties of modified aramid fibers by benzoquinolizine heterocycle. Journal Solid Rocket Techno, 35, 536-540.

Yang P., 2016, Study on rheological properties of mountains area coarse-- grained soil embankment and settlement prediction method, Chemical Engineering Transactions, 51, 1033-1038 DOI: 10.3303/CET1651173

Zavadskii A.E., 2011, Analysis of the Orientation of Supramolecular Structures in Fibers by the Method of X-Ray Diffractometry, Fibre Chem,43(3), 263-266.